Multiphoton Laser Scanning Microscopy on Non-Melanoma Skin Cancer: Morphologic Features for Future Non-Invasive Diagnostics

John Paoli[1], Maria Smedh[2], Ann-Marie Wennberg[1] and Marica B. Ericson[1,3]

This study describes the morphologic features of human non-melanoma skin cancer obtained using multiphoton laser scanning microscopy (MPLSM) on freshly excised specimens from 14 patients. Optical sectioning parallel to the tissue surface was performed, resulting in *en face* autofluorescence images of the epidermis and upper dermis, reaching tissue depths of 135 μm. The microscopy was carried out *ex vivo* using a femtosecond pulsed laser at 780 nm and a ×40/0.8 objective. The autofluorescence was detected in the range of 450–530 nm. Traditional histopathological criteria such as bowenoid dysplasia, multinucleated cells, or hyperkeratosis in squamous cell carcinoma *in situ* (SCCIS) (five specimens), and peripheral palisading of tumor cells in superficial basal cell carcinoma (SBCC) (six specimens) were clearly discerned. The morphologic features differed significantly between these lesions and perilesional skin. However, characteristic tumor aggregates were found in only one of the three investigated nodular basal cell carcinomas (NBCCs) due to limited imaging depth. In addition, speckled perinuclear fluorescence was observed in both lesions and normal perilesional skin. In conclusion, MPLSM could potentially be applied for non-invasive diagnostics of SCCIS and SBCC, whereas the ability to characterize NBCC is unclear at this point.

Journal of Investigative Dermatology (2008) **128,** 1248–1255; doi:10.1038/sj.jid.5701139; published online 8 November 2007

INTRODUCTION

The incidence of non-melanoma skin cancer, such as basal cell carcinoma (BCC) and squamous cell carcinoma, is a rising problem in most countries with a fair-skinned population (Diepgen and Mahler, 2002; Staples *et al.*, 2006). Today, the routine diagnostic procedure for BCC and squamous cell carcinoma is visual inspection followed by skin biopsy and subsequent histopathological examination. This invasive procedure is not only associated with pain but also with diagnosis delay and costly human resources. Therefore, there is a need to find faster and, if possible, non-invasive diagnostic procedures for these types of skin cancer, especially in their early stages.

The recent advances in imaging technology have enabled the development of new non-invasive diagnostic techniques. For example, dermoscopy has been used to identify pigmented BCCs (Menzies *et al.*, 2000), to visualize vascular structures in skin tumors (Argenziano *et al.*, 2004), and to study squamous cell carcinoma *in situ* (SCCIS) (Zalaudek *et al.*, 2004). Several other imaging methods have been applied to improve clinical demarcation of BCC tumor margins, including bispectral fluorescence imaging (Stenquist et al., 2006), spectrophotometric intracutaneuos analysis (Moncrieff *et al.*, 2002), terahertz pulsed imaging (Wallace *et al.*, 2004) and positron emission tomography (Fosko *et al.*, 2003). Unfortunately, these imaging tools mostly provide macroscopic information and lack histopathological confirmation of the tumor diagnosis, which can only be obtained using microscopy techniques.

Human skin is optically turbid, scattering, and absorbing visible light to a high degree (Richards-Kortum and Sevick-Muraca, 1996). Thus, conventional light microscopy is restricted to being performed on very thin tissue specimens. This obstacle may be overcome by novel microscopy techniques based on near-infrared (NIR) or infrared radiation, which lies in the so-called ''optical window'' (Anderson and Parrish, 1981) for biological tissue, because it is much less scattered and absorbed than other wavelength regions. For example, reflectance-mode confocal laser scanning microscopy (RCLSM) has been implemented for *in vivo* microscopy of human skin to obtain images of the epidermis and upper dermis comparable to routine histopathology (Rajadhyaksha *et al.*, 1999; Gonzalez *et al.*, 2003). It has also proven useful for imaging of BCC (Gonzalez and Tannous, 2002; Gerger

[1]*Department of Dermatology, Sahlgrenska University Hospital, Göteborg University, Göteborg, Sweden;* [2]*Centre for Cellular Imaging, Göteborg University, Göteborg, Sweden and* [3]*Department of Physics, Göteborg University, Göteborg, Sweden*

Correspondence: Dr John Paoli, Department of Dermatology, Sahlgrenska University Hospital, Göteborg 413 45, Sweden.
E-mail: john.paoli@vgregion.se

Abbreviations: BCC, basal cell carcinoma; DP, dermal papillae; MPLSM, multiphoton laser scanning microscopy; NADPH, nicotinamide adenine dinucleotide phosphate; NBCC, nodular basal cell carcinoma; NIR, near-infrared; RCLSM, reflectance-mode confocal laser scanning microscopy; SB, stratum basale; SBCC, superficial basal cell carcinoma; SC, stratum corneum; SCCIS, squamous cell carcinoma in situ*; SG, stratum granulosum; SS, stratum spinosum*

Received 8 March 2007; accepted 16 August 2007; published online 8 November 2007

et al., 2005a) and melanocytic lesions (Langley *et al.*, 2001; Gerger *et al.*, 2005b). Another related technique is multiphoton laser scanning microscopy (MPLSM), which is an advanced fluorescence microscopy technique (Denk *et al.*, 1990; Diaspro, 2002). In MPLSM, excitation of fluorophores is obtained by a nonlinear multiphoton process, as opposed to one-photon excitation used in conventional fluorescence microscopy. Two-photon excitation occurs when two photons, of approximately half the one-photon excitation energy, are absorbed practically simultaneously by the fluorescent molecule. This means that NIR radiation can be used to excite fluorophores, either endogenous autofluorescent substances or fluorescent markers added to the specimen, which normally are excited by UV or visible light. In order for the two-photon process to occur, high-intensity radiation from a femtosecond pulsed laser is required. Due to the nonlinearity, the excitation only occurs at the focal point and, therefore, images from a thin optical section can be obtained without using a pinhole. MPLSM can thus probe much deeper into biological tissue in comparison to conventional confocal fluorescence microscopy both due to the use of low-scattering, low-absorbing NIR excitation light and more effective emission detection. Two-dimensional, *en face* images are acquired through optical sectioning parallel to the tissue surface (ie, in the *x–y* plane). Three-dimensional images, called *z*-stacks, can be obtained by sequentially changing the plane of focus (*z*-level), thus scanning at different tissue depths. The MPLSM technique has successfully been applied to acquire high-resolution optical sections deep into thick, highly light-scattering, biologic tissues (Denk *et al.*, 1990), such as human skin (Masters *et al.*, 1997; Yu *et al.*, 2001; Konig and Riemann, 2003; Mulholland *et al.*, 2004).

The endogenous fluorescent biomolecules present in human skin include reduced nicotinamide adenine dinucleotide, nicotinamide adenine dinucleotide phosphate (NADPH), collagen, keratin, melanin, elastin, flavines, and lipofuscin (Kollias *et al.*, 2002; Konig and Riemann, 2003). These fluorophores generally require excitation wavelengths in the UV spectral range, which is highly energetic and damaging to the skin. Hence, excitation with NIR light, as in MPLSM, is less harmful for biological tissue and a clear advantage if used as an *in vivo* diagnostic method (Konig and Riemann, 2003). MPLSM potentially reduces the risk of photodamage to living cells, minimizes the photobleaching of endogenous fluorophores, and improves background discrimination (Masters and So, 1999).

The autofluorescence of human skin has been detected down to tissue depths of 100–200 μm using MPLSM (Konig and Riemann, 2003; Masters *et al.*, 2004). MPLSM has also been applied on human skin to study dermal penetration of drugs (Konig *et al.*, 2006; Luengo *et al.*, 2006; Stracke *et al.*, 2006) and skin aging (Lin *et al.*, 2005; Koehler *et al.*, 2006). The technique allows imaging of cellular and subcellular structures of the epidermis and upper dermis. MPLSM has the potential to become an *in vivo,* bedside, non-invasive, optical skin biopsy technique (Masters *et al.*, 1997; Konig and Riemann, 2003), which might facilitate the diagnostics of non-melanoma skin cancer in the future, avoiding the disadvantages of routine histopathology. In fact, a commercial product for *in vivo* MPLSM is already available (Konig and Riemann, 2003; Konig *et al.*, 2006). The technique has proven to be an effective tool in distinguishing normal, precancerous, and cancerous epithelial tissues in an *in vivo* cancerous hamster cheek pouch model (Skala *et al.*, 2005). Publications on MPLSM to visualize premalignant and malignant human skin tumors are, unfortunately, very limited. Until now, MPLSM has only been performed on thin cross-section slices of nodular BCC (NBCC) (Lin *et al.*, 2006). In order to take the technique into clinical reality, more information is required on how *en face* MPLSM images of human tumors should be interpreted in comparison to routine histopathology, and which diagnostic criteria can be identified using this technique. Hence, the aim of this study was to investigate and describe the morphologic and autofluorescent features found in *en face* MPLSM images of freshly excised human non-melanoma skin cancer and normal perilesional skin. The lesions studied were SCCIS, superficial BCC (SBCC) and NBCC obtained from 14 patients.

RESULTS

In this study, *en face* MPLSM images were collected *ex vivo* from freshly excised lesions and surrounding normal perilesional skin in five SCCIS, six SBCC, and three NBCC specimens. Series of two-dimensional images in the *x–y* plane, parallel to the skin surface, were obtained from the stratum corneum (SC) down to a maximum depth of 135 μm giving rise to three-dimensional image stacks, or *z*-stacks. The imaging was performed using a femtosecond pulsed laser operating at 780 nm and a ×40/0.8 water immersion objective. Emission from the skin was detected in the range of 450–530 nm, corresponding to the autofluorescence of nicotinamide adenine dinucleotide, NADPH, keratin, elastin, collagen, and melanin, allowing us to visualize the cellular structures within the epidermis and upper dermis of the specimens.

Normal perilesional skin

The morphologic features observed in all 14 specimens of normal perilesional skin using MPLSM *ex vivo* were similar to each other and agreed well with reports from other authors on MPLSM of normal skin studied *ex vivo* (Laiho *et al.*, 2005) and *in vivo* (Masters *et al.*, 1997; Konig and Riemann, 2003). Selected *en face* images at various tissue depths of one typical sample are shown in Figure 1a (Movie S1). The SC, mainly consisting of keratin, was highly fluorescent and its thickness varied between approximately 9 and 18 μm in the different samples. The outline of the large, flattened, anucleated corneocytes, representing the SC, could be discerned in the most superficial sections of all specimens.

Below the SC, in the sections corresponding to the stratum granulosum (SG), the cells were characterized by fluorescent cellular cytoplasms surrounding non-fluorescent round nuclei. The regularly distributed cells of the SG (23–25 μm in diameter) showed a weaker fluorescence than other epidermal cells, resulting in a lower overall fluorescent signal

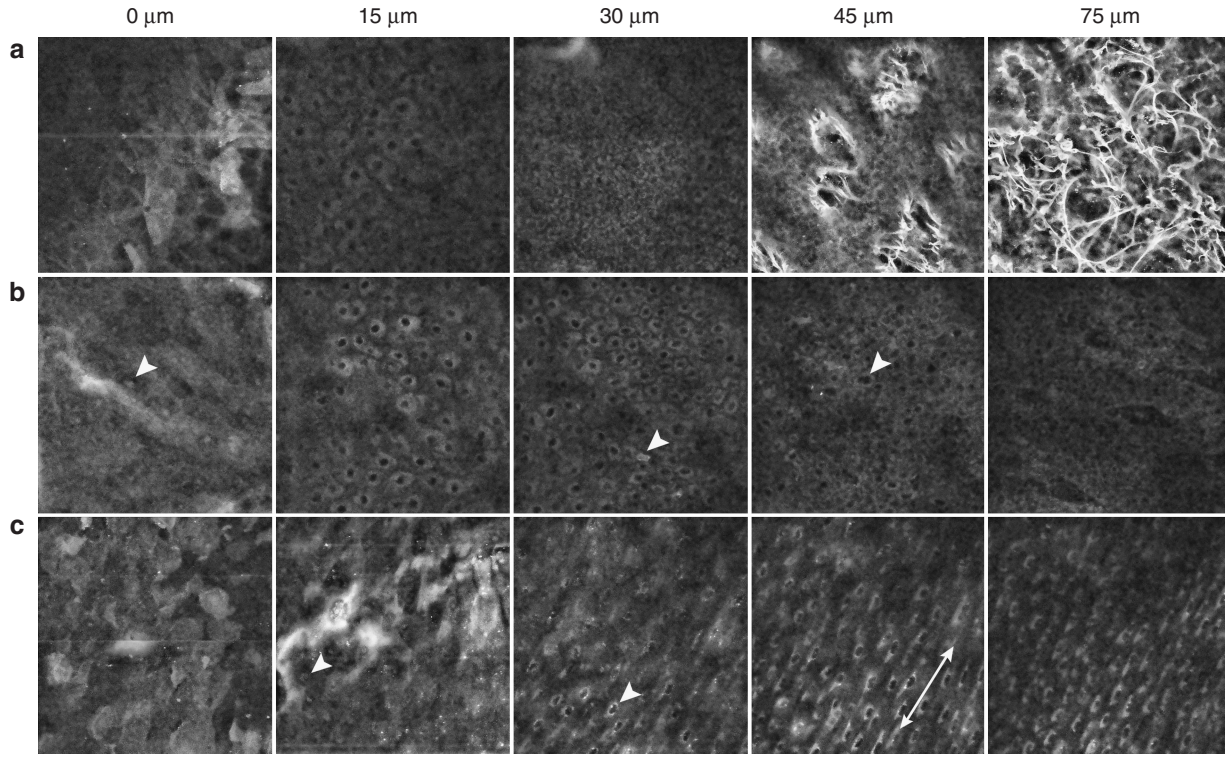

Figure 1. MPLSM images of normal perilesional skin, an SCCIS specimen, and an SBCC specimen. (**a**) In the normal perilesional skin, the SC (0 µm), the SS (15 µm), the SB (30 µm), the DP (45 µm), and the dermis (75 µm) are visualized. (**b**) This SCCIS sample shows fluorescent nuclei compartments within the SC (0 µm, arrow), the loss of cell polarity and widened intercellular spaces of the SG (15 µm), a dyskeratotic cell in the SS (30 µm, arrow), a multinucleated cell among the atypical cells of the SS/SB (45 µm, arrow) and the DP appearing at depths of 75 µm. (**c**) The corneocytes of the SBCC specimen at 0 µm appear normal but present fluorescent nuclei compartments at 15 µm (arrow); speckled perinuclear fluorescence is present among the keratinocytes at 30 µm (arrow) and elongated polarized nuclei are seen at 45 µm (double-pointed arrow) and 75 µm.

compared to the SC, the stratum spinosum (SS), and the stratum basale (SB).

The cytoplasmic autofluorescence increased notably with epidermal depth and the apical poles of the cuboidal cells of the SB were found to be very brightly fluorescent. As was expected, a gradual decrease in cell size down to a diameter of 12–15 µm was noted when imaging the SS down to the SB. In addition, the relation between the volume of the cytoplasms and the volume of the nuclei of the keratinocytes also decreased gradually with depth.

Cells within the SG, the SS, and the SB were homogeneously distributed and separated by thin non-fluorescent intercellular spaces. The epidermal cells and their nuclei showed regular shapes and sizes presenting no signs of cellular atypia. Bright, speckled perinuclear fluorescence among the keratinocytes of the SG and/or the SS was observed in 6 of 14 specimens of normal perilesional skin. This fluorescent feature has previously been described in MPLSM images of precancerous epithelial tissues in an *in vivo* hamster model (Skala *et al.*, 2005).

At depths of 35–45 µm, dark, rounded areas appeared in the images corresponding to the tips of the dermal papillae (DP). Within these areas, bright and highly fluorescent filaments were observed originating from thin, interlaced elastin and collagen fibers. Rounded or oval non-fluorescent structures corresponding to capillaries could be distinguished among the highly fluorescent fibers of the DP. The last keratinocytes of the SB within the rete ridges were observed at depths of 70–90 µm. Only connective tissue fibers surrounded by non-fluorescent stroma were visible beyond the rete ridges down to a maximum imaging depth of 135 µm.

Squamous cell carcinoma *in situ*

The MPLSM images acquired from the five SCCIS specimens differed significantly from those obtained from the corresponding normal perilesional skin specimens as summarized in Table 1. MPLSM images of a typical SCCIS sample are illustrated in Figure 1b (Movie S2). The SC was abnormally thick compared to the corresponding perilesional skin, up to 30–40 µm, in three of the SCCIS lesions. Within the same specimens, fluorescent nuclei compartments within the corneocytes were observed. This morphologic and fluorescent feature has been described earlier in the presence of hyperkeratosis (Konig and Riemann, 2003). In two hyperkeratotic lesions, large, rounded bundles of keratin were observed within the SC, corresponding to so-called keratin pearls.

In all but one lesion, the keratinocytes within the SG, the SS, and the SB were irregularly distributed, reflecting a loss of cell polarity. Dimly fluorescent and widened intercellular

Table 1. Morphologic features and fluorescent patterns observed in *en face* MPLSM images of SCCIS compared to the corresponding normal perilesional skin

Specimen number	1		2		3		4		5	
Morphologic feature	L	N	L	N	L	N	L	N	L	N
Bowenoid dysplasia[1]	+	−	−	−	+	−	+	−	+	−
Multinucleated cells	+	−	+	−	+	−	+	−	+	−
Widened intercellular spaces	−	−	−	−	+	−	+	−	+	−
Hyperkeratosis	+	−	+	+	+	−	+	−	−	−
Keratin pearls	+	−	−	−	−	−	+	−	−	−
Dyskeratosis[2]	+	−	−	−	+	−	−	−	−	−
Loss of cell polarity	+	−	−	−	+	−	+	−	+	−
Speckled perinuclear fluorescence	−	−	+	−	+	+	+	−	+	−

L, lesion; N, corresponding perilesional skin; +, present; −, not present.
[1]Defined as pleomorphism and substantial variation of nuclei size.
[2]Cells with brighter cytoplasmic fluorescence than the surrounding keratinocytes.

Table 2. Morphologic features and fluorescent patterns observed in *en face* MPLSM images of SBCC compared to the corresponding normal perilesional skin

Specimen number	1		2		3		4		5		6	
Morphologic feature	L	N	L	N	L	N	L	N	L	N	L	N
Hyperkeratosis	+	−	+	−	+	−	−	−	−	−	−	−
Thickened subcorneal epidermis	NA	−	+	−	+	−	+	−	+	−	+	−
Elongated cells and nuclei polarization	NA	−	+	−	−	−	−	−	−	−	−	−
Peripheral palisading	NA	−	−	−	−	−	−	−	+	−	+	−
Speckled perinuclear fluorescence	NA	−	+	+	+	+	+	−	+	+	+	+

L_1, lesion; N_1, corresponding perilesional skin; +, present; −, not present; NA, not applicable due to limited imaging depth.

spaces were present in three of these four lesions. Signs of bowenoid dysplasia, including pleomorphism and substantial variation of nuclei size (5–17 μm within single *z*-sections), were observed within the epidermis of four lesions. Large, multinucleated cells were noted in all five lesions.

Keratinocytes with brighter cytoplasmic fluorescence compared to surrounding cells in the SG and the SS were discerned in two lesions, possibly corresponding to dyskeratosis. Four lesions presented speckled perinuclear fluorescence in the SG and/or the SS, whereas this feature was only observed in one corresponding normal perilesional skin sample.

Superficial BCC

All of the six SBCC lesions showed a marked increase in epidermal thickness compared to their corresponding normal perilesional skin, as seen in Table 2, which summarizes the main morphologic and autofluorescent features found in the SBCC lesions and their corresponding normal perilesional skin. Hyperkeratosis was observed in three of six SBCC lesions. In one of these lesions, the hyperkeratosis was at least 60 μm thick and highly fluorescent, which hindered imaging of the underlying epidermis. Thus, other characteristic features were not discerned in this particular SBCC lesion. In four other lesions, the subcorneal epidermis was approximately twice as thick as in the corresponding normal perilesional skin. In these four lesions, the DP was still not visible at depths of 100–130 μm. In the last lesion, the DP could be visualized, but it appeared 10–15 μm deeper than in the corresponding normal perilesional skin.

The tumor cells were monomorphous and disposed in palisade in the periphery of two of the five lesions in which imaging was possible below the SC. In one lesion, the keratinocytes of the lower third of the epidermis presented elongated nuclei and cytoplasms, which were oriented in the same direction in the *x*–*y* plane, a feature described as nuclei polarization (Gonzalez and Tannous, 2002; Nori *et al.*, 2004). This feature is illustrated by the SBCC sample presented in Figure 1c (Movie S3). Speckled perinuclear fluorescence was observed in the subcorneal epidermis of all five lesions but was also present in the corresponding normal perilesional skin in four specimens.

Nodular BCC

All three NBCC lesions included in this study presented an apparently normal structure and cell distribution when investigated with MPLSM, resembling the images acquired from the corresponding normal perilesional skin. However, typical nodular aggregates of tumor cells were found within the dermis of one lesion, as illustrated in Figure 2. The tumor nests lacked contiguity with the overlying normal epidermis and, the basal cells within these nests presented large, oval nuclei, little cytoplasm and peripheral palisading. The autofluorescence of these cells was comparable to that of the cells found in the SB. In the other two lesions, the epidermis was slightly thickened (10–20 μm) compared to the corresponding samples of normal perilesional skin and the fluorescent signal began to weaken at depths of 90–100 μm. No morphologic features of NBCC tumor nests could be observed in these lesions due to the limited imaging depth. Speckled perinuclear fluorescence was observed within the SG and the SS of the normal perilesional skin in one of the specimens, but surprisingly not in any of the images of the lesions.

Follow-up

None of the fourteen patients showed signs of clinical recurrence during follow-up after 3–6 months.

DISCUSSION

This study reports on the morphologic features observed in MPLSM imaging performed *ex vivo* on fresh tissue specimens

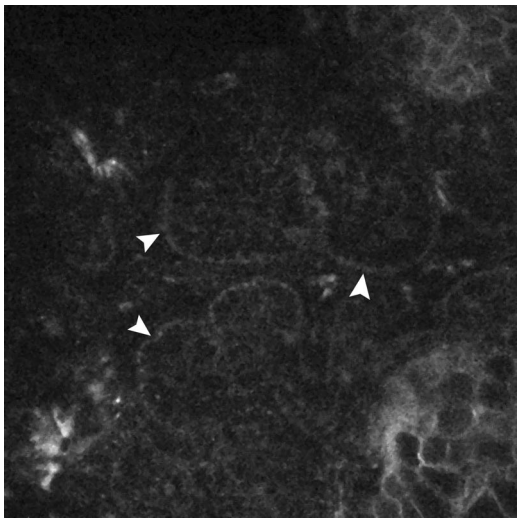

Figure 2. MPLSM image of an NBCC specimen at 70 μm. Notice the peripheral palisading of the basal cells (arrows) surrounding the typical nodular aggregates of tumor cells.

of non-melanoma skin cancer. The results show that traditional histopathological diagnostic criteria, such as bowenoid dysplasia, multinucleated cells, and hyperkeratosis in SCCIS and peripheral palisading of tumor cells in BCC, can clearly be observed using *en face* visualization of skin autofluorescence with MPLSM. The morphologic features differed significantly between the lesions and their corresponding perilesional skin in the cases of SCCIS and SBCC. However, in the case of NBCC a single significant feature (ie, the formation of tumor aggregates in the upper dermis) was found in only one of the three investigated lesions. This suggests that MPLSM could potentially be applied for non-invasive *in vivo* diagnostics of SCCIS and SBCC, whereas the ability to characterize NBCC is unclear at this point.

The MPLSM imaging of normal perilesional skin allows for the visualization of cellular and subcellular components of all four layers of the epidermis as well as the intricate network of fibers within the papillary dermis, as shown here and in other studies using MPLSM on normal skin *in vivo* (Masters *et al.*, 1997; Konig and Riemann, 2003). Nicotinamide adenine dinucleotide and NADPH have been reported to be the main source of autofluorescence from the keratinocytes of human skin and are present within cytoplasmic mitochondria (Kollias *et al.*, 2002). In this study, the mitochondria appeared as punctuated fluorescent organelles, in agreement with previous reports (Masters *et al.*, 1998; Konig and Riemann, 2003). In addition, the autofluorescence was observed to be the lowest in the SG and increasing when imaging deeper into the skin specimen until reaching the SB. Transmission electron microscopy studies on bovine rumen epithelium have shown that cytoplasmic mitochondrial density is the greatest in the apical pole of the SB cells, decreasing gradually in the SS and the SG, whereas mitochondria essentially are not present in the SC (Graham and Simmons, 2005). This is consistent with the theory that mitochondrial nicotinamide adenine dinucleotide and NADPH are the main origin of cytoplasmic fluorescence from the epidermal cells observed with MPLSM, and also explains the fluorescence distribution in the samples. Speckled perinuclear fluorescence was not detected in the SC, most likely explained by the lack of mitochondria. However, the corneocytes in the SC showed elevated fluorescence due to the high content of fluorescent keratin. Also the collagen and elastin fibers in the DP were highly fluorescent, in agreement with other reports (Masters and So, 1999; Konig and Riemann, 2003).

Other authors have described the MPLSM imaging of collagen present in dermis originating from the phenomenon of second harmonic generation (Konig and Riemann, 2003; Laiho *et al.*, 2005). This is a nonlinear scattering process in which two photons combine to form a single photon of exactly half the wavelength. However, the second harmonic generation, expected at 390 nm (when using 780 nm excitation), was not observed, as the choice of filter setting in our study was 450–530 nm. Thus, the recorded MPLSM images in this study correspond solely to visualization of autofluorescence in the dermis.

The morphologic features of SCCIS as observed by MPLSM in this study, included bowenoid dysplasia (ie, pleomorphism and substantial variation of nuclei size), multinucleated cells, loss of cell polarity, widened intercellular spaces, hyperkeratosis, keratin pearls, dyskeratosis, and speckled perinuclear fluorescence. All features, with the exception of the speckled perinuclear fluorescence, correlate well with the atypia of SCCIS seen in routine histopathology (McKee and Brenn, 2005). The presence of speckled perinuclear fluorescence has previously been reported in precancerous epithelial tissues in a hamster model explained by the NADPH fluorescence of perinuclear mitochondria (Skala *et al.*, 2005). In our study, however, this fluorescence pattern was also observed in the upper epidermis of several samples of normal perilesional skin, as well as in SBCC lesions. This suggests that speckled perinuclear fluorescence may be a sign of actinic damage. Furthermore, this sign could theoretically also be due to an increased amount of keratohyalin granules. Therefore, the presence or absence of this fluorescent pattern must be studied in other dermatologic entities before it is used as a diagnostic criterion when performing MPLSM on human skin tumors.

The characteristic features found in the SBCC lesions were increased thickness of the subcorneal epidermis, peripheral palisading of tumor cells in the lower epidermis, and speckled perinuclear fluorescence in the upper epidermis. In one lesion, we observed elongated cells and nuclei polarization in the lower third of the epidermis, which has earlier been described in SBCC lesions using RCLSM *in vivo* (Gonzalez and Tannous, 2002; Nori *et al.*, 2004; Gerger *et al.*, 2005a). It is not possible to completely exclude the possibility of elongated cells, nuclei polarization, and presence of peripheral palisading at deeper tissue layers in the other five lesions due to the limited imaging depth.

Visualization of the cellular structures of NBCCs with MPLSM proved to be difficult, also due to the limited imaging depth. Nodular aggregates of basal cells with peripheral palisading within the dermis, comparable to the typical histopathological presentation (McKee and Brenn, 2005),

were observed in only one of the three NBCC specimens. The maximum imaging depth achieved in this study was 135 μm. The use of more sensitive detectors, optimal filters, and more recent technology may improve the possibility of increasing imaging depth, which is of great importance in order to make MPLSM a possible diagnostic tool, even for NBCC.

Generally, when performing MPLSM on these human skin samples, the autofluorescent signal was rather weak and the laser power had to be increased when focusing deeper into the specimens due to loss of signal. There is a trade-off between laser power, detector gain, and scan rate in order to acquire high-contrast MPLSM images without causing thermal damage to the tissue. Tissue damage during MPLSM has previously been reported, particularly, the formation of cavitation at the epidermal–dermal junction (Masters *et al.*, 2004). The parameter settings applied in our study were on the limit of what was tolerated by the tissue. Only small increases in the laser power caused severe damage to the SC with tissue cavitation at the focal plane. Thus, it is of great importance to evaluate carefully the safety aspects of the technique before performing *in vivo* measurements on patients.

MPLSM has the potential to be used as a diagnostic method for superficial precancerous and cancerous lesions of the human skin. Theoretically, it is minimally invasive and does not depend on labeling dyes or pretreatment of samples, making it an ideal technique for *in vivo* diagnosis (Lin *et al.*, 2006). There are several other research groups currently developing techniques for *in vivo* measurements on humans (Masters *et al.*, 2004; Koehler *et al.*, 2006; Konig *et al.*, 2006). Both MPLSM and RCLSM can be used to image human skin at a subcellular level. MPLSM with NIR light has been shown to provide enhanced contrast when imaging corneocytes in the SC, dermal collagen, and elastin, whereas RCLSM with visible light has the advantage of less complex instrumentation (Masters and So, 1999). However, there are, to our knowledge, no comparative studies on MPLSM and RCLSM with NIR light. In this study, we have shown that several diagnostic criteria can be visualized using MPLSM on SCCIS and SBCC specimens. On the other hand, our present MPLSM set-up presented difficulties in characterizing NBCCs, mainly due to limitation in imaging depth. Hence, further refinement of the technique is needed to make it a reliable diagnostic tool. The image acquisition procedure must be made faster and more sensitive to allow for *in vivo* investigations. In addition, the possibility of thermal mechanical damage must be safely controlled, in order to bring MPLSM into clinical practice.

MATERIALS AND METHODS

Patients and tissue sampling

The local ethics committee granted approval of the study protocol before the start of this study. The Declaration of Helsinki Principles was followed and all patients gave written, informed consent prior to inclusion. In total, 14 patients with histopathologically verified BCC and SCCIS were included. All lesions measured more than 6 mm in diameter and had well-defined borders to ensure complete removal. Patients with lesions located on the face or in the genital area were excluded. All lesions were removed surgically by standard local excision with at least a 3 mm margin. A follow-up of all patients was carried out after 3–6 months to ensure that the lesions had not recurred.

In total, 14 specimens of normal perilesional skin, five SCCIS specimens, three specimens of NBCC, and six of SBCC were investigated using MPLSM. Image stacks from 29 different areas of normal perilesional skin, 12 areas within the SCCIS specimens, 4 areas in the NBCC specimens, and 19 areas in the SBCC specimens were obtained.

Specimen preparation

The tissue specimens excised contained the entire skin lesion and normal perilesional skin from the ends of the spindle-shaped resection. Directly following the surgical removal of each specimen, two biopsies were taken from the bulk of the tumor and from normal perilesional tissue, respectively, using a 6-mm diameter dermal biopsy punch (Miltex Inc., York, PA). These biopsies were trimmed from subcutaneous tissue with surgical scissors. The remaining full-thickness skin biopsies containing epidermal and dermal tissue were then moistened with a few drops of phosphate-buffered saline (8.5 g l^{-1} NaCl; 0.36 g l^{-1} $NaH_2PO_4 \cdot 2H_2O$; 1.37 g l^{-1} $Na_2HPO_4 \cdot 2H_2O$; pH 7.2–7.4). The biopsies were placed in a 20 mm diameter and 1 mm deep imaging chamber gasket (CoverWell™, Invitrogen™, Eugene, OR) with the skin surface against the cover slip. A microscope slide (Menzel-Gläser, Menzel GmbH, Braunschweig, Germany) was subsequently adhered to the imaging chamber to enable imaging by MPLSM. The slides with the prepared specimens were then wrapped in aluminium foil to protect them from light and stored in a refrigerator at 6–8°C/43–46°F until MPLSM was performed. All imaging was completed within 4–6 hours after excision.

Imaging instrumentation

The MPLSM of *ex vivo* human skin was performed at the Centre for Cellular Imaging, Göteborg University, Göteborg, Sweden. The confocal laser *x–y* scanning microscope system was a Bio-Rad Radiance 2100MP Rainbow (Bio-Rad, Hemel Hempstead, UK; company purchased by Carl Zeiss in 2004) built on an inverted Olympus IX71 microscope (Olympus, Hamburg, Germany). A pulsed femtosecond titanium-sapphire laser (Tsunami®, Spectra-Physics, Mountain View, CA) with a 10 W Millennia Xs pump source provided the excitation light. The wavelength of the laser was tuned to 780 nm. At this wavelength, a pump power of 8.5 W resulted in an output power from the Tsunami of around 1.8 W. The emitted autofluorescence was collected through a ×40 water-immersion lens with a 0.8 numerical aperture and a working distance of 1.7 mm (Carl Zeiss C Achroplan NIR ×40/0.8). The emission was detected in the wavelength region of 450–530 nm by an internal descanned photomultiplier tube with a fully opened pinhole. A signal-enhancing lens was placed in front of the pinhole in order to collect as much of the scattered emission as possible. The signal-enhancing lens therefore provided non-confocal detection by the internal detectors and signal strengths comparable to the non-descanned external set-up (Amos, 2000).

The collected *z*-series consisted of several *en face* image planes parallel to the skin surface (*x–y* sections) from all specimens. Images were obtained from the surface of the epithelium down to a

maximum depth of 135 μm. Each *x–y* section comprised a scan area of 323 × 323 μm (512 × 512 pixels). A total of 4–8 scans of each *x–y* section were averaged by Kalman filtering (Kalman, 1960) to improve the image quality. The steps between the adjacent *x–y* sections in the *z*-series ranged from 1 to 10 μm. As the tissue depth increased, the laser power was increased by changing the transmission through the Pockels cell between approximately the values 10–100 of the laser power control in the LaserSharp software. This corresponds to a power of approximately 10–270 mW at the back aperture of the objective, which has a transmission of about 80% at 780 nm, as measured with a power meter (model 407A, Spectra Physics, Mountain View, CA).

Evaluation of morphology and fluorescence

The MPLSM images were evaluated using the ImageJ 1.34s (National Institutes of Health) and MatLab (MathWorks Inc., Natick, MA) software. The images were noise-reduced through bilateral filtering (Tomasi and Manduchi, 1998) and further enhanced by using the method for contrast-limited adaptive histogram equalization in the MatLab imaging toolbox. This allowed for visual inspection of various morphologic features and fluorescence patterns of cellular and subcellular components within normal perilesional skin and the skin lesions.

CONFLICT OF INTEREST

The authors state no conflict of interest.

ACKNOWLEDGMENTS

This study was financed by grants from the federal government under the ALF agreement. We acknowledge the Centre for Cellular Imaging, Göteborg University, for the use of imaging equipment and support from the staff. We also thank histopathologist Dr Lena Mölne for her guidance during image interpretation, Adaocha Odu for her help with image processing and, finally, research nurse Christina Halldin for taking such good care of our patients.

SUPPLEMENTARY MATERIAL

Movie S1. A typical MPLSM image stack of normal perilesional skin.

Movie S2. A typical MPLSM image stack of SCCIS presenting hyperkeratosis, bowenoid dysplasia, as well as dyskeratotic and multinucleated cells.

Movie S3. An MPLSM image stack of SBCC presenting hyperkeratosis, a thickened subcorneal epidermis, speckled perinuclear fluorescence, elongated cells and nuclei polarization.

REFERENCES

Amos WB (2000) Optimum optical design characteristics for confocal and multi-photon imaging systems. Bio-Rad Technical Note 09. 1–8

Anderson RR, Parrish JA (1981) The optics of human skin. *J Invest Dermatol* 77:13–9

Argenziano G, Zalaudek I, Corona R, Sera F, Cicale L, Petrillo G *et al.* (2004) Vascular structures in skin tumors: a dermoscopy study. *Arch Dermatol* 140:1485–9

Denk W, Strickler JH, Webb WW (1990) Two-photon laser scanning fluorescence microscopy. *Science* 248:73–6

Diaspro A (2002) Confocal and Two-Photon Microscopy: Foundations, Applications and Advances. New York: Wiley-Liss Inc., 567 pp

Diepgen TL, Mahler V (2002) The epidemiology of skin cancer. *Br J Dermatol* 146(Suppl 61):1–6

Fosko SW, Hu W, Cook TF, Lowe VJ (2003) Positron emission tomography for basal cell carcinoma of the head and neck. *Arch Dermatol* 139:1141–6

Gerger A, Horn M, Koller S, Weger W, Massone C, Leinweber B *et al.* (2005a) Confocal examination of untreated fresh specimens from basal cell carcinoma: implications for microscopically guided surgery. *Arch Dermatol* 141:1269–74

Gerger A, Koller S, Kern T, Massone C, Steiger K, Richtig E *et al.* (2005b) Diagnostic applicability of *in vivo* confocal laser scanning microscopy in melanocytic skin tumors. *J Invest Dermatol* 124:493–8

Gonzalez S, Swindells K, Rajadhyaksha M, Torres A (2003) Changing paradigms in dermatology: confocal microscopy in clinical and surgical dermatology. *Clin Dermatol* 21:359–69

Gonzalez S, Tannous Z (2002) Real-time, *in vivo* confocal reflectance microscopy of basal cell carcinoma. *J Am Acad Dermatol* 47: 869–874

Graham C, Simmons NL (2005) Functional organization of the bovine rumen epithelium. *Am J Physiol Regul Integr Comp Physiol* 288:R173–81

Kalman RE (1960) A new approach to linear filtering and prediction problems. *Trans ASME J Basic Eng* 82:35–45

Koehler MJ, Konig K, Elsner P, Buckle R, Kaatz M (2006) *In vivo* assessment of human skin aging by multiphoton laser scanning tomography. *Opt Lett* 31:2879–81

Kollias N, Zonios G, Stamatas GN (2002) Fluorescence spectroscopy of skin. *Vib Spectrosc* 28:17–23

Konig K, Ehlers A, Stracke F, Riemann I (2006) *In vivo* drug screening in human skin using femtosecond laser multiphoton tomography. *Skin Pharmacol Physiol* 19:78–88

Konig K, Riemann I (2003) High-resolution multiphoton tomography of human skin with subcellular spatial resolution and picosecond time resolution. *J Biomed Opt* 8:432–9

Laiho LH, Pelet S, Hancewicz TM, Kaplan PD, So PT (2005) Two-photon 3-D mapping of *ex vivo* human skin endogenous fluorescence species based on fluorescence emission spectra. *J Biomed Opt* 10:024016

Langley RG, Rajadhyaksha M, Dwyer PJ, Sober AJ, Flotte TJ, Anderson RR (2001) Confocal scanning laser microscopy of benign and malignant melanocytic skin lesions *in vivo*. *J Am Acad Dermatol* 45:365–76

Lin SJ, Jee SH, Kuo CJ, Wu RJ, Lin WC, Chen JS *et al.* (2006) Discrimination of basal cell carcinoma from normal dermal stroma by quantitative multiphoton imaging. *Opt Lett* 31:2756–8

Lin SJ, Wu R Jr, Tan HY, Lo W, Lin WC, Young TH *et al.* (2005) Evaluating cutaneous photoaging by use of multiphoton fluorescence and second-harmonic generation microscopy. *Opt Lett* 30:2275–7

Luengo J, Weiss B, Schneider M, Ehlers A, Stracke F, Konig K *et al.* (2006) Influence of nanoencapsulation on human skin transport of flufenamic acid. *Skin Pharmacol Physiol* 19:190–7

Masters BR, So PT (1999) Multi-photon excitation microscopy and confocal microscopy imaging of *in vivo* human skin: a comparison. *Microsc Microanal* 5:282–9

Masters BR, So PT, Buehler C, Barry N, Sutin JD, Mantulin WW *et al.* (2004) Mitigating thermal mechanical damage potential during two-photon dermal imaging. *J Biomed Opt* 9:1265–70

Masters BR, So PT, Gratton E (1997) Multiphoton excitation fluorescence microscopy and spectroscopy of *in vivo* human skin. *Biophys J* 72:2405–12

Masters BR, So PT, Gratton E (1998) Multiphoton excitation microscopy of *in vivo* human skin. Functional and morphological optical biopsy based on three-dimensional imaging, lifetime measurements and fluorescence spectroscopy. *Ann N Y Acad Sci* 838:58–67

McKee PH, Brenn T (2005) Tumors of the surface epithelium. In: *Pathology of the Skin – With Clinical Correlations* (McKee PH, Calonje JE, Granter SR, eds), Edinburgh: Elsevier, 1153–240

Menzies SW, Westerhoff K, Rabinovitz H, Kopf AW, McCarthy WH, Katz B (2000) Surface microscopy of pigmented basal cell carcinoma. *Arch Dermatol* 136:1012–6

Moncrieff M, Cotton S, Claridge E, Hall P (2002) Spectrophotometric intracutaneous analysis: a new technique for imaging pigmented skin lesions. *Br J Dermatol* 146:448–57

Mulholland WJ, Kendall MA, White N, Bellhouse BJ (2004) Characterization of powdered epidermal vaccine delivery with multiphoton microscopy. *Phys Med Biol* 49:5043–58

Nori S, Rius-Diaz F, Cuevas J, Goldgeier M, Jaen P, Torres A *et al.* (2004) Sensitivity and specificity of reflectance-mode confocal microscopy for *in vivo* diagnosis of basal cell carcinoma: a multicenter study. *J Am Acad Dermatol* 51:923–30

Rajadhyaksha M, Gonzalez S, Zavislan JM, Anderson RR, Webb RH (1999) *In vivo* confocal scanning laser microscopy of human skin II: advances in instrumentation and comparison with histology. *J Invest Dermatol* 113:293–303

Richards-Kortum R, Sevick-Muraca E (1996) Quantitative optical spectroscopy for tissue diagnosis. *Annu Rev Phys Chem* 47:555–606

Skala MC, Squirrell JM, Vrotsos KM, Eickhoff JC, Gendron-Fitzpatrick A, Eliceiri KW *et al.* (2005) Multiphoton microscopy of endogenous fluorescence differentiates normal, precancerous, and cancerous squamous epithelial tissues. *Cancer Res* 65:1180–6

Staples MP, Elwood M, Burton RC, Williams JL, Marks R, Giles GG (2006) Non-melanoma skin cancer in Australia: the 2002 national survey and trends since 1985. *Med J Aust* 184:6–10

Stenquist B, Ericson MB, Strandeberg C, Molne L, Rosen A, Larko O *et al.* (2006) Bispectral fluorescence imaging of aggressive basal cell carcinoma combined with histopathological mapping: a preliminary study indicating a possible adjunct to Mohs micrographic surgery. *Br J Dermatol* 154:305–9

Stracke F, Weiss B, Lehr CM, Konig K, Schaefer UF, Schneider M (2006) Multiphoton microscopy for the investigation of dermal penetration of nanoparticle-borne drugs. *J Invest Dermatol* 126:2224–33

Tomasi C, Manduchi R (1998) Bilateral filtering for gray and color images. *Proceedings of the 1998 IEEE International Conference on Computer Vision*, Bombay, 839–46

Wallace VP, Fitzgerald AJ, Shankar S, Flanagan N, Pye R, Cluff J *et al.* (2004) Terahertz pulsed imaging of basal cell carcinoma *ex vivo* and *in vivo*. *Br J Dermatol* 151:424–32

Yu B, Dong CY, So PT, Blankschtein D, Langer R (2001) *In vitro* visualization and quantification of oleic acid induced changes in transdermal transport using two-photon fluorescence microscopy. *J Invest Dermatol* 117:16–25

Zalaudek I, Argenziano G, Leinweber B, Citarella L, Hofmann-Wellenhof R, Malvehy J *et al.* (2004) Dermoscopy of Bowen's disease. *Br J Dermatol* 150:1112–6